Dislocationmechanicsbased constitutive relations for material dynamics calculations

Frank J. Zerilli and Ronald W. Armstrong

Citation: J. Appl. Phys. **61**, 1816 (1987); doi: 10.1063/1.338024
View online: http://dx.doi.org/10.1063/1.338024
View Table of Contents: http://jap.aip.org/resource/1/JAPIAU/v61/i5
Published by the American Institute of Physics.

Dislocation-mechanics-based constitutive relations for material dynamics calculations

Frank J. Zerilli and Ronald W. Armstrong[a)]
Naval Surface Weapons Center, White Oak, Silver Spring, Maryland 20903-5000

(Received 25 August 1986; accepted for publication 7 November 1986)

An improved description of copper- and iron-cylinder impact (Taylor) test results has been obtained through the use of dislocation-mechanics-based constitutive relations in the Lagrangian material dynamics computer program EPIC-2. The effects of strain hardening, strain-rate hardening, and thermal softening based on thermal activation analysis have been incorporated into a reasonably accurate constitutive relation for copper. The relation has a relatively simple expression and should be applicable to a wide range of fcc materials. The effect of grain size is included. A relation for iron is also presented. It also has a simple expression and is applicable to other bcc materials but is presently incomplete, since the important effect of deformation twinning in bcc materials is not included. A possible method of accounting for twinning is discussed and will be reported on more fully in future work. A main point made here is that each material structure type (fcc, bcc, hcp) will have its own constitutive behavior, dependent on the dislocation characteristics for that particular structure.

I. INTRODUCTION

A. EPIC-2's constitutive relations

Johnson and Cook[1,2] have successfully described cylinder impact (Taylor) test results for a variety of materials by using the Lagrangian material dynamics code EPIC-2. A single type of numerical constitutive relationship was employed in the code, giving the von Mises yield stress as follows:

$$\sigma = (A + B\epsilon^n)(1 + C \ln \dot{\epsilon})(1 - T^{*m}), \qquad (1)$$

where $\dot{\epsilon}$ is the strain rate, and A, B, n, C, and m are material constants; T^* is the ratio $(T-T_{\text{room}})/(T_{\text{melt}}-T_{\text{room}})$, and T is the absolute temperature. The material constants were determined from limited straining tests done in tension or torsion. Strain hardening, strain-rate hardening, and thermal softening are taken into account.

B. Dislocation mechanics and improved constitutive relations

An improvement of the constitutive relations for individual materials being tested was imagined to lead to a better hydrocode[3] description of the experimental cylinder impact results. For example, OFHC (oxygen-free high conductivity) copper (99.99% Cu) and Armco iron, two of the materials tested by Johnson and Cook, are known to show different effects of straining on the strain rate and temperature dependencies of the flow stress. These dependencies are essentially independent of strain for Armco iron while they increase strongly with strain for OFHC copper. Furthermore, considerable research has been done in recent years to develop the dislocation-mechanics basis for describing constitutive relations, particularly for metals and alloys, following from the direct observation of the velocity dependence on stress of dislocations in lithium fluoride.[4] A review may be found in the monograph by Kocks, Argon, and Ashby.[5] Application of this body of knowledge to the hydrocode description of cylinder impact tests is important in two respects: first, the deformation theory can be assessed under test conditions not fully described by simple analytic calculations nor included in other standard testing procedures; second, a much better material-dependent constitutive equation description is provided than heretofore generally available in hydrocodes.

C. High strain rates and large strains

In regard to the first point (testing the theory), the original work of Taylor,[6] while providing an insight into the dynamics of the cylinder impact, provides only a very limited description of material strength (that is, the concept of dynamic yield strength). As researchers beginning with Taylor have noted,[6–9] while there is a straightforward correlation between the final-length/original-length ratio and an effective dynamic yield stress, it is practically impossible to predict the deformed shape of the cylinder using either a simple analytic model or a hydrocode model that does not take into consideration the real behavior of materials in regard to strain, strain rate, and thermal effects. The attempt to model a Taylor cylinder impact can provide a real test of a material model, since conditions of strain and strain-rate are achieved which are outside the range of ordinary testing—in particular, strain rates in the range of 10^4–10^6 s^{-1} and strains in the range of 0–2.

D. Need for improved constitutive relations

The material strength descriptions in hydrocodes have been generally limited to simple models, for example, elastic perfectly plastic, and elastic-plastic with linear work hardening. At best the models include work hardening, strain-rate dependence, and thermal softening, but the model is only a numeric fit to test data. There is no justification for relying

a) Permanent address: Department of Mechanical Engineering, University of Maryland, College Park, MD 20742.

on the models outside the limited range of the test data. Often the behavior of the models is at variance with the known behavior of materials (particularly in regard to the variation of strain-rate dependence with temperature). Generally, no account is taken of grain size although it is known that this will have a dramatic effect on the strength and ductility of materials. For example, the cylinder impact data for OFHC copper reported by Wilkins and Guinan[7] differ by about ten percent from that reported by Johnson and Cook[1,2]—the disparity is probably attributable to grain size and annealing differences. A code model based on Johnson–Cook copper would not give correct results for Wilkins–Guinan copper. Further, material models in codes generally take no account of the radically differing behavior of face-centered cubic materials like copper, and body-centered cubic materials like iron.

E. Preview

We will address the above issues in the following sections. Section II describes the Taylor test, Sec. III the dislocation-mechanics based constitutive relations model, and Sec. IV the detailed results obtained for copper and iron. As will be discussed, the results for copper are an unambiguous improvement over previous models—and the constants can be adjusted for grain size. The results for iron are more ambiguous but even more interesting. They indicate the necessity for including an additional physical phenomenon which is especially important in bcc materials—replacement of plastic flow by slip with plastic flow by deformation twinning. It should be emphasized that the constants for the models were obtained from a combination of theoretical considerations and test data independent of the cylinder impact tests. Sec. V summarizes the work and discusses future directions for study.

II. THE TAYLOR TEST

A. Deformation of a cylindrical projectile

In the test which bears his name, Taylor[6] proposed to measure the dynamic yield strength of iron from the deformation of cylindrical projectiles fired at a flat rigid target. If we assume that a good approximation to a rigid target can be achieved in practice, then the model is particularly easy to simulate numerically with a computer code. In addition, strains of the order of one or more are achieved together with strain rates of the order of 10^4–10^6 s^{-1}. The temperature rise in the material during impact can be several hundred degrees Kelvin. Thus, conditions are achieved in such a test which lie outside the range of normal static testing. The ability of a code to model a Taylor test should therefore be a good test of the constitutive relations to be described in Sec. III.

B. Longitudinal strain, yield stress, and kinetic energy

Several significant features which emerge from Taylor's original (1947) analysis are useful to review. If L_1 is the final length of the projectile and L_0 is the original length, then the ratio L_1/L_0 is a function only of $\rho U^2/2S$, the ratio of initial kinetic energy density to effective yield stress S (U is the initial impact velocity). Also, the duration time Δt of the plastic deformation, expressed in the dimensionless form $U\Delta t/L_0$, is a function only of $\rho U^2/2S$. This implies that the average strain rate in the projectile is inversely proportional to the initial length. The equations are independent of the diameter of the projectile. The L_1/L_0 ratio predicted by Taylor is verified in experiments, but the overall shape of the deformed projectile is not predicted well at all.

C. Mean strain, yield stress, and kinetic energy

In 1968, Hawkyard, Eaton, and Johnson,[9] noting the poor correlation of experimental with predicted shapes, took another approach. They noted that, typically, 99% of the initial kinetic energy of the projectile is converted into plastic work. We see this by noting that the residual elastic energy density w_E is less than $S^2/2E$, where S is an effective yield stress and E is Young's modulus. The ratio $2w_E/\rho U^2$ is less than 0.01 for impact velocities greater than 100 m/s for copper (taking $S\sim 300$ MPa) and 160 m/s for iron (taking $S\sim 600$ MPa). Since practically all of the kinetic energy is converted to plastic work, the effective yield stress S can be very simply related to the mean (cross-sectional) areal strain ϵ_m by equating the kinetic energy to the plastic work of deformation:

$$S\epsilon_m = \tfrac{1}{2}\rho U^2, \tag{2}$$

where

$$\epsilon_m = \frac{1}{V}\int \epsilon\, dV.$$

In particular, if $r(z)$ is the radius of the deformed cylinder as a function of distance z along the axis from the impacted end, then

$$\epsilon_m = \frac{2\int_0^{L_1} r^2 \ln(r/r_0)\,dz}{\int_0^{L_1} r^2\,dz}, \tag{3}$$

where r_0 is the radius of the undeformed cylinder.

D. Experiments and code calculations

In 1972, Wilkins and Guinan[7] reported a series of experiments for several metals (most notably, aluminum, tantalum, and steel), which tended to verify that the ratio L_1/L_0 is independent of initial length and diameter, and that the ratio scales as $\rho U^2/2S$ where S is approximately constant. They also modeled the impacts with a computer code and found that they could correlate the L_1/L_0 ratio with a constant S for many materials, copper being a notable exception. However, the radial deformation could not be predicted unless work hardening was included in the code model.

Wilkins and Guinan described an analytic model which is a simplification of Taylor's model. This model is described in Appendix A.

For the typical range of experiments, the time duration of impact can be estimated from $U\Delta t/L_0 \sim \rho U^2/2S$. As described in Appendix A, this gives a result which is within 30% of Taylor's result if $\frac{1}{8} < \rho U^2/2S < 1$.

Erlich and Chartagnac[10] have reported measurements of the radial deformation in 4340 steel cylinders impacted in symmetric end-on-end tests. A hypothetical composite stress-strain curve consisting of a linear work-hardening portion followed by a perfectly plastic portion was derived to

fit the experiment. However, no independent check was made to determine whether the derived stress-strain curve could predict the results of an experiment under different conditions.

III. CONSTITUTIVE RELATION MODEL

A. Thermal activation analysis

The dislocation model basis for determining the plastic shear strain-rate $\dot{\gamma}$ stems from the relationship

$$\dot{\gamma} = m' b N v \,, \tag{4}$$

where m' is a tensor orientation factor, N is the dislocation density, b is the Burgers vector, and v is the average dislocation velocity.[11] At an upper limiting dislocation velocity, near to the elastic shear wave speed, Nv is replaced by the alternative product of factors $\dot{N}\Delta x$, where Δx is the average dislocation displacement and $\dot{N}$ is the rate of increase of the dislocation density.[12] The overriding effect of dislocation generation has been demonstrated for elastic wave attenuation in shocked lithium fluoride crystals,[13] following from the pioneering work of Johnston and Gilman.[4] At lower velocities, however, v is determined by thermally activated overcoming of local obstacles to dislocation motion so that

$$v = v_0 \exp(-G/kT) \,. \tag{5}$$

In Eq. (5), v_0 is the reference dislocation velocity, G is the shear stress-dependent Gibbs free energy of activation, k is Boltzmann's constant, and T is the absolute temperature.

The activation energy G may be expressed in the form

$$G = G_0 - \int_0^{\tau_{\rm th}} A^* b \, d\tau'_{\rm th} \,, \tag{6}$$

where G_0 is the reference Gibbs energy at $T = 0$, A^* is the area of activation, and $\tau_{\rm th}$ is the thermal component of the shear stress. The physical dimensions of A^* may be used to characterize the thermal activation process. The mean value of $A^* b$, given by

$$Ab = \langle A^* \rangle b = \left(\frac{1}{\tau_{\rm th}}\right) \int_0^{\tau_{\rm th}} A^* b \, d\tau'_{\rm th} \,, \tag{7}$$

may be used for the same purpose.

The constitutive relationship involving the combined thermal activation strain-rate analysis parameters described in Eqs. (4)–(7) may be expressed in an alternative form, this time in terms of the uniaxial stress $\sigma_{\rm th} = m\tau_{\rm th}$, and strain $\epsilon = \gamma/m$, as[14]

$$\sigma_{\rm th} = B e^{-\beta T} \,, \tag{8}$$

where

$$B = m G_0 / A_0 b \tag{9}$$

and

$$\beta = (1/T) \ln(A/A_0) - (1/T) \times \ln[1 + (kT/G_0) \ln(\dot{\epsilon}/\dot{\epsilon}_0)] \,. \tag{10}$$

A_0 is the dislocation activation area at $T = 0$, m' and m are orientation factors, and $\dot{\epsilon}_0 = (m'/m) b N v_0$. Experimentally,[15]

$$\beta = \beta_0 - \beta_1 \ln(\dot{\epsilon}/\dot{\epsilon}_0) \,, \tag{11}$$

that is, the first term on the right side of Eq. (10) is effectively constant. Using the expansion $\ln(1 + x) \sim x$ for the second term, we see that $\beta_1 = k/G_0$.

Equation (11) is consistent with the thermodynamic basis for Eq. (5) as may be seen from a comparison of terms in Eq. (8) and Eq. (4). The comparison gives

$$G = (k/\beta_1) \ln(\tau_{\rm th0}/\tau_{\rm th}) - k(\beta_0/\beta_1) T \,, \tag{12}$$

where $\tau_{\rm th0}$ is the extrapolated value of the thermal component of shear stress at $T = 0$. The shear stress and temperature dependent terms in Eq. (12) correspond to the enthalpy and entropy terms, respectively, contained in the Gibbs free energy of activation. Note that $G = 0$ at $T = 0$.

B. Behavior of body centered cubic metals

A stronger dependence of the plastic yield stress on temperature and strain rate is known to result for body centered cubic (bcc) metals as compared with face centered cubic (fcc) metals. A very significant difference in behavior between the two structure types occurs in the experimental dependency on strain of the thermal activation analysis parameter A^*. For reasonably pure iron, molybdenum, niobium, and related bcc metals, A^* is essentially independent of plastic strain.[15] This observation has led to the interpretation that the intrinsic Peierls stress associated with the movement of a single dislocation is responsible for the thermal activation analysis behavior.[16] Consequently, $\sigma_{\rm th}$ can be written without regard for the strain from Eqs. (8)–(11) as

$$\sigma_{\rm th} = c_1 \exp(-c_3 T + c_4 T \ln \dot{\epsilon}) \,. \tag{13}$$

C. Behavior of face-centered cubic metals

For copper, aluminum, and related fcc metals, the thermal activation analysis behavior is strongly dependent on strain, and this has led to the interpretation that the intersection of dislocations is the controlling mechanism for the thermal activation analysis behavior.[17] On this basis, the activation area A^* is a measure of the separation distance d between points of dislocation intersection, according to the relationship

$$A^* \simeq d b / 2 \,. \tag{14}$$

However d is also related to the dislocation density by the relationship

$$N \sim 1/d^2 \,, \tag{15}$$

and, in turn, the multiple slip-crystal flow stress at any value of strain is connected in general both to N and ϵ by the relations[18,19]

$$\sigma_0 \simeq \sigma'_0 (b/d) \simeq \sigma''_0 \epsilon^{1/2} \,. \tag{16}$$

Presuming that the approximate Eqs. (14)–(16) may be employed to determine A_0 at $T = 0$, then

$$A_0 = A'_0 \epsilon^{-1/2} \,, \tag{17}$$

and thus, for the fcc metal case, the strain, temperature, and strain rate combine to determine $\sigma_{\rm th}$ as

$$\sigma_{\rm th} = c_2 \epsilon^{1/2} \exp(-c_3 T + c_4 T \ln \dot{\epsilon}) \,. \tag{18}$$

The separate plastic strain-hardening contribution to the flow stress of reasonably pure bcc metals may be evaluat-

ed from an assumed power law dependence on strain given by

$$\Delta\sigma_G = c_5\epsilon^n , \tag{19}$$

where c_5 and n are experimental constants as described for the first factor in Eq. (1).

D. Influence of solute and grain size

For both bcc and fcc metals, an additional component of stress, $\Delta\sigma'_G$, potentially occurs for the influence of solute and the original dislocation density on the yield stress. Also, for bcc, fcc, and other structure types, the polycrystal flow stress is raised at relatively low temperatures due to the requirement of slip band-stress concentrations at grain boundaries being needed for the transmission of plastic flow between the polycrystal grains.[20] This consideration leads to an incremental stress $\Delta\sigma$ being given by the product of a microstructural stress intensity k and the inverse square root of the average grain diameter l:

$$\Delta\sigma = kl^{-1/2} . \tag{20}$$

The k values for bcc metals showing a definite yield point are significantly larger than those for fcc metals. There is some strain dependence of k.

E. The fcc and bcc constitutive relations

The foregoing description of stress components which combine to determine the plastic flow stresses of bcc or fcc metals leads to two separate reasonably explicit expressions for their constitutive behavior. In the fcc case,

$$\sigma = \Delta\sigma'_G + c_2\epsilon^{1/2}\exp(-c_3T + c_4T\ln\dot{\epsilon}) + kl^{-1/2} . \tag{21}$$

A main consideration is that the temperature softening and strain-rate hardening dependence of σ are greater with increased strain hardening. For the bcc case,

$$\sigma = \Delta\sigma'_G + c_1\exp(-c_3T + c_4T\ln\dot{\epsilon}) + c_5\epsilon^n + kl^{-1/2} . \tag{22}$$

Beyond the uncoupled strain hardening factor from the strain-rate hardening and thermal softening dependencies for this case, these latter dependencies and the grain size dependence as well are generally larger than those corresponding dependencies exhibited by fcc metals.

F. Constants for the constitutive relations

The constants for the constitutive relations for copper [Eq. (21)] and iron [Eq. (22)] are listed in Table I, based mainly on the experimental results of Johnson and Cook.[1,2] For both metals, tensile data covering a range of strain 0.0–0.3 were available at temperatures of 300, 500, and 735 K.

1. Constants for copper

Consider first the case for copper. A graph of $\ln\sigma_\epsilon$ vs T at a fixed strain ϵ of 0.3 was employed to estimate, by subtraction of various stress increments, a combined value for $\Delta\sigma'_G + kl^{-1/2}$ of 65 MPa. Then $\ln(\sigma_\epsilon - 65\ \text{MPa})$ was plotted versus T for the several strains 0.01, 0.10, and 0.30. The intercepts of lines of constant slope were employed for the three flow stress curves at the three increasing strain values to determine σ_ϵ values at $T = 0$ of 105, 265, and 495 MPa, respectively. A plot of these σ_ϵ values versus $\epsilon^{1/2}$ gave a value for c_2 of 890 MPa. At 300 K, torsion data were available for shear strain rates $\dot{\gamma}$ in the range 0.1–148 s^{-1}. Since $\epsilon = \ln(1 + \gamma/\sqrt{3})$, a graph of

$$\ln(\sigma_{0.456} - 65\ \text{MPa})\ \text{vs}\ \ln[\dot{\gamma}/\sqrt{3}(1 + \gamma/\sqrt{3})]$$

was employed for $\gamma = 1 (\epsilon = 0.456)$ to determine a value for c_4 of 0.000 115 K^{-1}. For $\dot{\epsilon} = 1.0\ s^{-1}$, a value of $\sigma_{0.456}$ was estimated from the graph and, from that value, a value for c_3 of 0.0028 K^{-1} was then computed directly from Eq. (21). A value for k of 5.0 $N/mm^{3/2}$ was obtained from the results of Hansen and Ralph,[21] and a mean value of $l^{-1/2}$ of 3.7 $mm^{-1/2}$ was obtained from Johnson and Cook to give a value of 18.5 MPa for $kl^{-1/2}$. Subtracting this from 65 MPa gives 46.5 MPa for $\Delta\sigma'_G$.

TABLE I. Constants for the dislocation-mechanics-derived constitutive relations for OFHC copper (fcc structure) [Eq. (21)], and Armco iron (bcc structure) [Eq. (22)].

Parameter	OFHC copper	Armco iron
$\Delta\sigma'_G$ (MPa)	46.5	0.0
c_1 (MPa)	···	1033
c_2 (MPa)	890	···
c_3 (K^{-1})	0.002 8	0.006 98
c_4 (K^{-1})	0.000 115	0.000 415
c_5 (MPa)	···	266.0
n	···	0.289
k ($MPa\ mm^{1/2}$)	5	22.0

2. Constants for iron

A similar procedure was followed for iron [Eq. (22)] except that account was taken of the separation of strain hardening from the combined temperature and strain-rate dependencies of the flow stress. On this basis, in examining the temperature dependence of the flow stress, values of $\Delta\sigma'_G + kl^{-1/2} + c_5\epsilon^n$ of 138 and 260 MPa were subtracted from σ_ϵ at strains of 0.01 and 0.30, respectively. A value of 1033 MPa for c_1 was determined at $T = 0$. From plots of

$$\ln(\Delta\sigma'_G + kl^{-1/2} + c_5\epsilon^n)$$

vs $\ln\epsilon$, a value of 65 MPa was estimated for $\Delta\sigma'_G + kl^{-1/2}$. With 22 $N/mm^{3/2}$ for k from Armstrong[20] and 3.0 $mm^{-1/2}$ for $l^{-1/2}$ from Johnson and Cook,[1,2] $\Delta\sigma'_G$ is approximately zero. The strain hardening constants were determined to be 266 MPa for c_5 and 0.289 for n. The strain-rate dependence was determined from a comprehensive plot of $\ln(\sigma_{ly} - k_1l^{-1/2})$ vs $\ln\dot{\epsilon}$ for EN2 steel as reported by Campbell, Cooper, and Fischhof,[22] where σ_{ly} is the lower yield stress. Their data indicated that k_1 is 22.4 $N/mm^{3/2}$ and $l^{-1/2}$ is 6.25 $mm^{-1/2}$. From the strain rate dependence, c_4 is determined to be 0.000 415 K^{-1} and therefore, from Eq. (13), c_3 is 0.006 98 K^{-1}. As mentioned earlier, the temperature and strain-rate dependencies of the flow stress for iron are significantly greater than those for copper as now may be seen from a comparison of the c_3 and c_4 coefficients in the two cases.

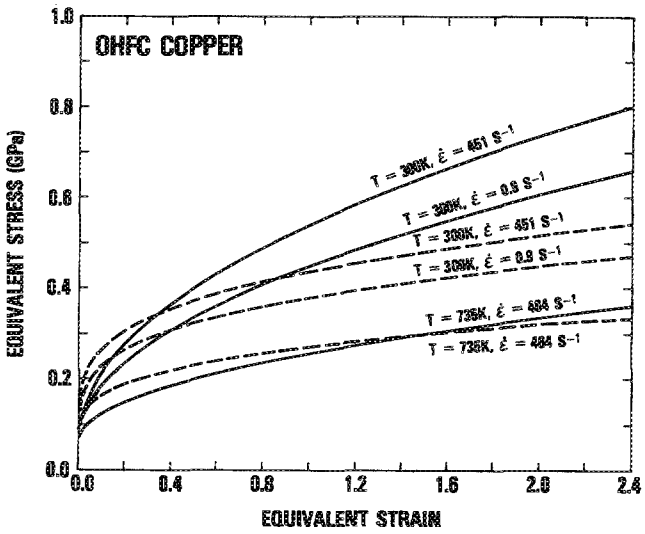

FIG. 1. Isothermal stress-strain curves for OFHC copper. The solid lines are plotted from Eq. (21) using the parameters in Table I, while the dashed lines are plotted from Eq. (1) using the parameters given in Refs. 1 and 2 ($A = 90$ MPa, $B = 292$ MPa, $n = 0.31$, $C = 0.025$, and $m = 1.09$).

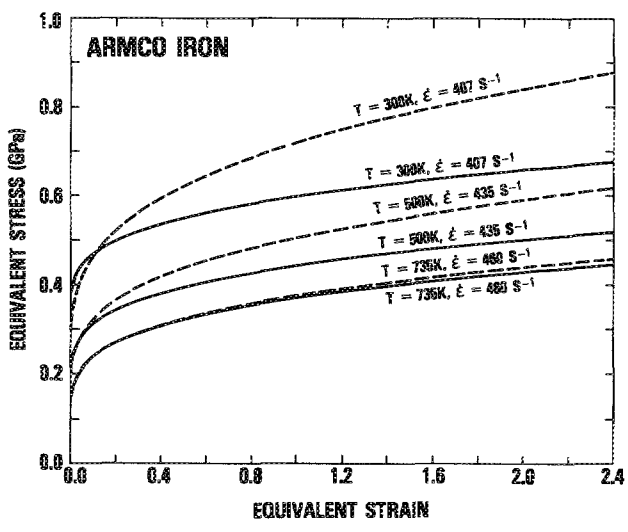

FIG. 2. Isothermal stress-strain curves for Armco iron. The solid lines are plotted from Eq. (22) using the parameters in Table I, while the dashed lines are plotted from Eq. (1) using the parameters given in Refs. 1 and 2 ($A = 175$ MPa, $B = 380$ MPa, $n = 0.32$, $C = 0.060$, and $m = 0.55$).

TABLE II. Comparison of experimental data of Johnson and Cook with stress-strain behavior predicted by Eqs. (1) and (21) for copper and Eqs. (1) and (22) for iron. Constants for the dislocation-mechanics-based Eqs. (21) and (22) are from Table I. The experimental data were provided by Johnson (see also Johnson and Cook, Ref. 2, Fig. 3). Constants for Eq. (1) are from Johnson and Cook, Ref. 2, Table II. For OFHC copper: $A = 90$ MPa, $B = 292$ MPa, $n = 0.31$, $C = 0.025$, and $m = 1.09$. For Armco iron, $A = 175$ MPa, $B = 380$ MPa, $n = 0.32$, $C = 0.060$, and $m = 0.55$.

OFHC copper					
T (K)	$\dot{\epsilon}$ (s^{-1})	ϵ	σ experiment (MPa)	σ, Eq. (21) (MPa)	σ, Eq. (1) (MPa)
294	451	0.01	110	113	184
294	451	0.10	200	217	268
294	451	0.30	340	328	335
493	449	0.01	110	97	154
493	449	0.10	190	165	225
493	449	0.30	280	238	281
730	464	0.01	90	84	114
730	464	0.10	140	126	167
730	464	0.30	200	171	208
Armco iron					
T (K)	$\dot{\epsilon}$ (s^{-1})	ϵ	σ experiment (MPa)	σ Eq. (22) (MPa)	σ Eq. (1) (MPa)
294	407	0.01	397	411	357
294	407	0.10	469	478	486
294	407	0.30	535	529	590
496	435	0.01	192	248	240
496	435	0.10	298	315	326
496	435	0.30	371	366	397
733	460	0.01	143	175	177
733	460	0.10	212	242	241
733	460	0.30	275	293	293

G. Stress-strain curves

Computed isothermal stress-strain curves are shown for several temperatures and strain rates representative of the input tests employed to establish the constitutive relations for copper (Fig. 1) and for iron (Fig. 2). Despite the tensile strain limitation of ϵ less than 0.30 having been employed by Johnson and Cook[1,2] to establish the stress-strain behavior, the computed curves have been carried to strains of about two in anticipation of the range of strains involved in the Taylor test results. The trends for copper in Fig. 1 are clear, showing, on the basis of the present analysis, appreciable strain hardening and an increasing strain-rate hardening, and thermal softening dependence of the flow stress with increasing strain, as may be confirmed by reference to indications from the original data obtained by Johnson and Cook.[1,2] For iron (Fig. 2), the newly described stress-strain behavior reflects the separation of the strain hardening and combined strain-rate hardening and thermal softening behaviors, again, as indicated in the stress-strain results reported by Johnson and Cook.[1,2] The single constitutive relation, Eq. (1), employed by Johnson and Cook, is seen to give an intermediate behavior between that of copper and that of iron, as should be expected. Interestingly enough, the stress-strain behavior of copper at a strain value of approximately one is seen to give an isothermal temperature dependence comparable to the (strain-independent) isothermal temperature dependence of iron. However, as will be seen, the stress-strain behavior at these strain (and stress) levels would normally be expected to be very nearly adiabatic (for example, in a Taylor test), and this produces very significant differences between copper and iron (whose behavior becomes essentially adiabatic at very much smaller strains). A comparison of the experimental and predicted stress-strain behavior for copper and iron is given in Table II.

TABLE III. Comparison of cylinder impact simulations with experimental results for OFHC copper, average grain size 0.075 mm, initial length $L_0 = 25.4$ mm, initial radius $R_0 = 3.81$ mm. L_1 is the final length of the cylinder and R_1 is the final radius of the impacted end. The numbers in parentheses are the percent deviation from the experimental values.

Impact velocity	Experimental result		Simulation using Eq. (1)		Simulation using dislocation-mechanics-based Eq. (21)	
(m/s)	L_1/L_0	R_1/R_0	L_1/L_0	R_1/R_0	L_1/L_0	R_1/R_0
130	0.770	1.30	0.812(+ 5)	1.48(+ 13)	0.784(+ 2)	1.41(+ 8)
146	0.736	1.40	0.778(+ 6)	1.58(+ 13)	0.750(+ 2)	1.49(+ 6)
190	0.638	1.78	0.682(+ 7)	1.92(+ 8)	0.658(+ 3)	1.77(− 0)

IV. RESULTS AND DISCUSSION

A. Cylinder tests

Johnson and Cook published data for cylinder impact tests of OFHC copper, Armco iron, and 4340 steel, and they used these data to evaluate the EPIC-2 code constitutive relations. In order to test the constitutive relations described in Eqs. (21) and (22), we incorporated those relations in the EPIC-2 code and compared the results both to the experimental data (kindly provided by Johnson) and also to the simulations done by Johnson and Cook. Table III summarizes the results for OFHC copper and Table IV summarizes the results for Armco iron. Table V summarizes the maximum von Mises equivalent strains and the maximum temperatures predicted by the EPIC-2 code using Eqs. (21) and (22). The maximum strain rates achieved are in excess of 10^5 s^{-1}. Taking a typical example, the 221 m/s iron impact, elements in about half the original cylinder length suffered strain rates greater than 10^4 s^{-1}, and elements in the first tenth of the cylinder see strain rates greater than 10^5 s^{-1}.

B. Results for copper

The results for copper shown in Table III indicate a significant improvement in the predictions using the dislocation-mechanics-based constitutive relations [Eq. (21)] as compared with EPIC-2's built-in relations [Eq. (1)]. This is illustrated more clearly in Fig. 3, in which the radial strain [log(radius/initial radius)] is plotted versus axial position for the experimental results and for the two code model results for the 190 m/s impact. The code model using the dislocation-mechanics-based relations shows a distinctly better correlation with the experimental results. Figure 4 compares the deformed cylinder outlines produced by the code models with the experimental results. Contours of von Mises equivalent strain are also shown in Fig. 4. The magnitudes of the strains range up to about two and are greater at the periphery as expected. The results for the other velocities are very similar to those for the 190 m/s impact and are not reproduced here.

From Figs. 3 and 4 we may deduce that the Johnson–Cook relations for copper are too soft at large strains and too hard at small strains. The dislocation-mechanics-based relations are very slightly soft at large strains and a little bit hard at small strains, but in general seem to reproduce the material behavior reasonably well.

C. Results for iron

The results for iron shown in Table IV do not indicate a significant difference in accuracy between the Johnson–Cook relations [Eq. (1)], and the dislocation-mechanics-based constitutive relations [Eq. (22)]. This is surprising, since the dislocation-mechanics-based relations provide a better fit to the low-strain rate test data. In general, Eq. (1) exhibits more work hardening than is evident in the experimental data (for example, see Table II and Ref. 2, *op.cit.*, Fig. 3). The models of the three impacts using Eq. (1) underpredict the final length. The models using Eq. (22) go from overprediction at 197 m/s to underprediction at 279 m/s. Examination of Fig. 5, in which is plotted radial strain versus axial position for the 221 m/s impact, indicates that both constitutive relations are too soft at large strains, while the Johnson–Cook relations are too soft also at small strains

TABLE IV. Comparison of cylinder impact simulations with experimental results for Armco iron, average grain size 0.120 mm, initial radius $R_0 = 3.81$ mm. The initial length L_0 for the 197 and 221 m/s tests was 25.4 mm, and for the 279 m/s test it was 12.6 mm. L_1 is the final length of the cylinder and R_1 is the final radius of the impacted end. The numbers in parentheses are the percent deviation from the experimental values.

Impact velocity	Experimental result		Simulation using Eq. (1)		Simulation using dislocation-mechanics-based Eq. (22)	
(m/s)	L_1/L_0	R_1/R_0	L_1/L_0	R_1/R_0	L_1/L_0	R_1/R_0
197	0.802	1.59	0.795(− 1)	1.65(+ 4)	0.816(+ 2)	1.66(+ 5)
221	0.780	1.80	0.755(− 3)	1.80(− 0)	0.779(− 0)	1.81(+ 0)
279	0.707	1.97	0.664(− 6)	1.92(− 3)	0.691(− 2)	1.86(− 6)

TABLE V. Maximum von Mises equivalent strains and temperatures predicted by EPIC-2, using dislocation-mechanics-based constitutive relations [Eqs. (21) and (22)].

Material	Velocity (m/s)	ϵ_{max}	T_{max} (K)	$\dot{\epsilon}_{max}$ (s^{-1})
Cu	130	0.0	140	···
Cu	146	1.1	440	···
Cu	190	1.8	570	···
Fe	197	1.6	610	···
Fe	221	2.0	680	4×10^5
Fe	279	2.0	720	···

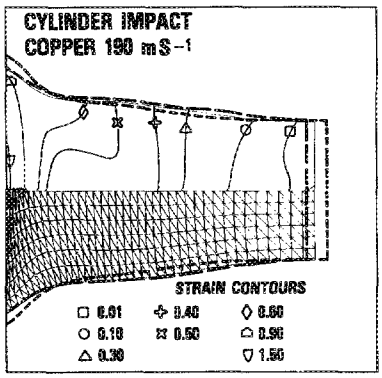

FIG. 4. Deformed cylinder outline, mesh, and contours of von Mises equivalent strain using the dislocation dynamics constitutive relations [Eq. (21)], in EPIC-2 for the 190 m/s copper cylinder impact (solid lines). The long-dashed line is the experimental result, and the short-dashed line is the results of the computation based on Eq. (1).

(leading to underprediction of length), and the dislocation-mechanics-based relations are a little bit too hard at small strains. Figure 6, which displays the experimental and computed deformed cylinder outlines, illustrates the same features.

D. Deformation twinning

Since the strain rates at the high strain end are between 10^4 and 10^5 s^{-1} with accompanying stresses of approximately 600–800 MPa, it is surmised that plastic flow by slip is being replaced by flow by deformation twinning. This would make the material harder at the large strain end of the cylinder and would be in the right direction to improve the model prediction for iron, perhaps to the same extent as occurred in the case of copper (where twinning should be unimportant).

In fact, an examination of enlargements of photomicrographs provided by Johnson shows unambiguous evidence of extensive twinning in all three impact samples. These results illustrate the pitfalls of attempting to extrapolate low strain-rate test data outside the range of the data.

E. Support for the twinning hypothesis

In the original studies by Taylor and colleagues, Carrington and Gaylor[23] reported that for a mild steel cylinder of diameter 8.9 mm and length 12.5 mm impacting at a velocity of 155 m/s, deformation twinning had occurred. A twinning stress of 690 MPa was indicated in the work of Campbell, Cooper, and Fischhof[22] to be achieved at an extrapolated strain rate of 10^4 s^{-1} at 293 K. Twinning was also observed for lower strain rates at lower temperatures. The twinning stress is essentially athermal but is generally associated with very significant work hardening of the material[24]; consequently, the expectation would be that the onset of deformation twinning would cause the material to behave as though it were stronger than otherwise predicted, very much in line with the experimental results of Johnson and Cook.

F. Twinning in the elastic precursor?

An interesting conjecture is that the twinning may occur at the elastic wave front and propagate with it by continued nucleation so long as the necessary stress level is maintained. Rohde[25] concluded that the dynamic yield stress of Ferrovac E iron in shock wave experiments was controlled by deformation twinning. This would produce an effective grain-size refinement, and so an effectively strengthened material which would then undergo further permanent deformation by slip in the follow-on plastic wave. With a reduced amount

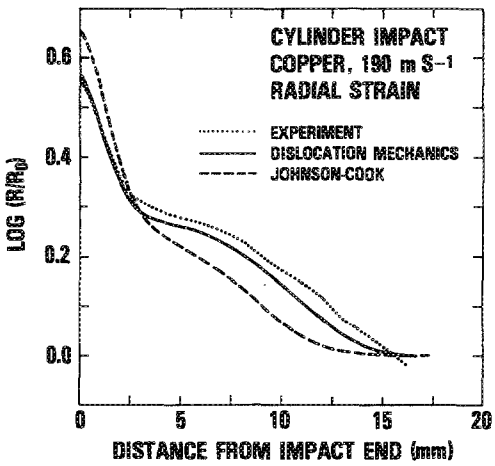

FIG. 3. The radial strain vs distance from the impacted end for the 190 m/s copper-cylinder impact test. The dotted line is the experimental result of Johnson and Cook, the dashed line is the EPIC-2 simulation result based on Eq. (1), and the solid line is the EPIC-2 simulation result based on dislocation-mechanics-derived Eq. (21).

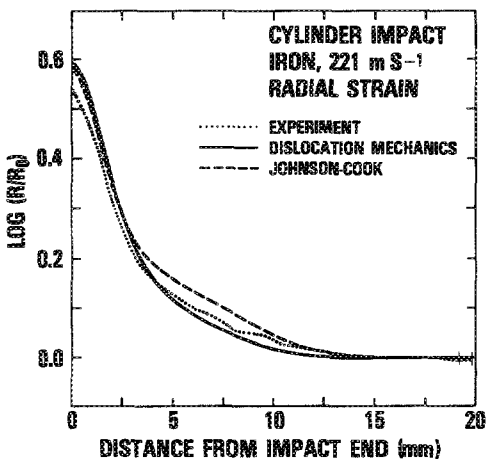

FIG. 5. The radial strain vs distance from the impacted end for the 221 m/s iron cylinder impact test. The dotted line is the experimental result of Johnson and Cook, the dashed line is the EPIC-2 simulation result based on Eq. (1), and the solid line is the EPIC-2 simulation result based on dislocation-mechanics-derived Eq. (22).

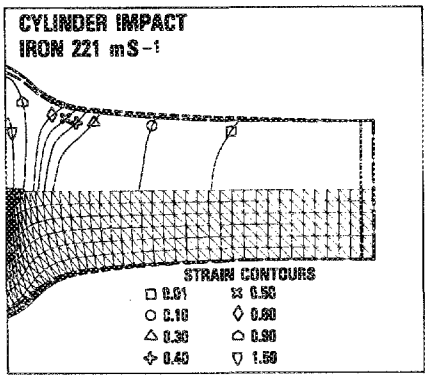

FIG. 6. Deformed cylinder outline, mesh, and contours of von Mises equivalent strain using the dislocation dynamics constitutive relations [Eq. (22)] in EPIC-2 for the 221 m/s iron cylinder impact (solid lines). The long-dashed line is the experimental result, and the short-dashed line is the result of the computation based on Eq. (1).

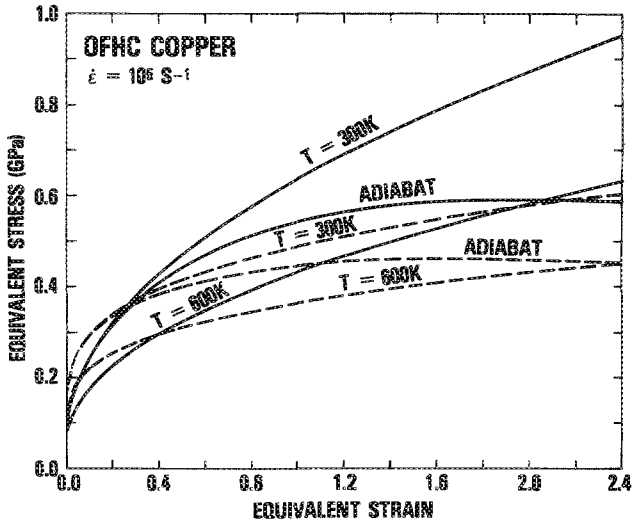

FIG. 7. Stress-strain curves for OFHC copper at a strain rate of 10^5 s^{-1}. The solid lines are plotted from the dislocation-mechanics-based constitutive relations [Eq. (21)] using the parameters in Table I. The dashed lines are plotted from Eq. (1) using the parameters given in Refs. 1 and 2 ($A = 90$ MPa, $B = 292$ MPa, $n = 0.31$, $C = 0.025$, and $m = 1.09$). The 300 and 600 K isotherms are shown, as well as an adiabat starting at 300 K initial temperature.

of twinning to be expected as the essentially elastic wave propagates along the cylinder (and hence, a reduced amount of effective grain size refinement), the true constitutive relation applicable to the Taylor test result would be raised significantly at the impact end and less so at larger distances from it, very much in agreement with the needed modification to the computed results shown in Fig. 5. A related type of behavior to that proposed here has in fact been proposed for shock-loaded copper by Warnes, Karpp, and Follansbee.[26] For their studies of an explosively expanded copper ring test, it was argued that the forerunning shock produced a severely strain-hardened material which was then subjected to the follow-on plastic wave front.

G. Relating the adiabatic stress-strain curve to the deformation of an element

The foregoing discussion leads to the further consideration of the extent to which the input constitutive data and consequent relations may be matched with the deformation behavior of elements in the code model description. Plastic strain rates on the order of 10^5 s^{-1} are experienced by the most deformed elements near the copper- or iron-cylinder periphery at the impact surfaces. Figures 7 and 8 show stress-strain curves relevant to these elements. Figure 7 compares copper behavior in the Johnson–Cook and dislocation-mechanics models. After a strain of about 0.3, the adiabatic curve begins to depart significantly from the 300 K isotherm, crossing the 600 K isotherm at a strain of about 2, nearly the strain reached in the 190 m/s impact. Note that 0.3 is the final strain actually achieved in the input testing procedure. Concentrating our attention on the dislocation-mechanics-derived curves, we see that the temperature softened stress-strain curve shows an effectively reduced strain hardening behavior, but still one far from being well represented by an elastic-perfectly plastic material response, such as might be envisioned for the determination of the dynamic yield stress by preceding investigators. Figure 8, however, shows a more striking behavior for the influence of thermal softening on the behavior of iron. Again, concentrating on the dislocation-mechanics-derived curves, we see that the onset of thermal softening occurs earlier because of the initially high value of the plastic flow stress. The behavior is closer to an elastic-perfectly plastic response at low strains and the flow stress decreases at larger strains above about 0.2. Looking back now at Fig. 5, we can see that the code model results using the dislocation-mechanics-based relations, compared to the results using the Johnson–Cook relation, are just what we would expect from an examination of the adiabatic stress-strain curves shown in Fig. 8.

H. Low temperature versus high strain-rate adiabatic behavior

The adiabatic behavior shown in the dislocation-mechanics-derived curve in Fig. 8 corresponds very well with

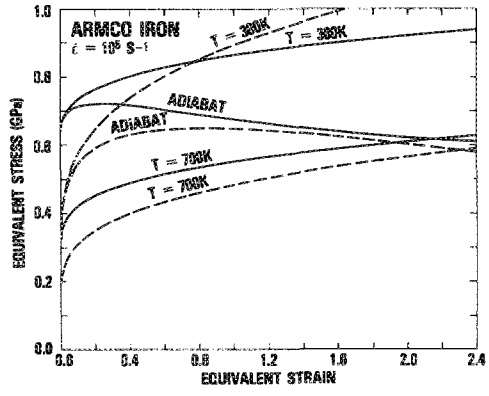

FIG. 8. Stress-strain curves for Armco iron at a strain rate of 10^5 s^{-1}. The solid lines are plotted from the dislocation-mechanics-based constitutive relations [Eq. (22)], using the parameters in Table I. The dashed lines are plotted from Eq. (1) using the parameters given in Refs. 1 and 2 ($A = 175$ MPa, $B = 380$ MPa, $n = 0.32$, $C = 0.060$, and $m = 0.55$). The 300 and 700 K isotherms are shown, as well as an adiabat starting at 300 K initial temperature.

the type of behavior reported as far back as 1943 by Zener and Hollomon in their study of the effect of strain rate on the plastic flow of steel.[27] In verifying the equivalence of increase of strain rate with decrease of temperature, they noted that at low temperatures the adiabatic curves had an initial negative slope. Equation (22) has just this behavior in the limit of low temperatures or high strain rates, as would be seen by plotting a sequence of adiabatic curves for successively lower initial temperatures. In fact, the Zener–Hollomon relation for describing the coupled temperature and strain-rate dependencies of the flow stress of iron was arrived at with reasoning similar to the dislocation-mechanics analysis leading to Eq. (22).

V. SUMMARY AND FUTURE WORK

A. Summary

In summary, the dislocation-mechanics-derived constitutive relations fit the test data for copper with improved accuracy, and have led to new insight into the importance of deformation twinning for understanding the mechanical properties of iron. It is important that failure of the consitutive relations for slip in iron to describe the high deformation-rate behavior led to the question of whether twinning might have occurred, and this was confirmed by subsequent observations. The constitutive relations have a theoretical basis, and so provide the possibility of evaluation of parameters from first principles. They naturally provide for the differentiation between fcc (copper) and bcc (iron) deformation behavior, and they may be extrapolated with greater reliability. At the same time, they may be incorporated into hydrocodes with virtually the same ease as numerically fitted functions. The reliability of the equations allows a closer examination of the correspondence of code calculations to experimental results.

B. Study of fracture

The successful result of using dislocation-mechanics-derived constitutive relations to model the permanent deformation behavior of copper and the promise that inclusion of twinning into the constitutive relation will lead to equally successful results for iron leads to the possibility of deriving successful damage and fracture models. Both damage and fracture depend critically on the stress and strain locally, so that constitutive relations which describe materials only in an average sense are not likely to lead to successful fracture modeling. The dislocation-mechanics-based relations offer the possibility of accurately predicting the strain, stress, strain rate, and temperature at a point with sufficient accuracy to improve the current status of fracture modeling. In the final analysis, the dislocation-based description is intimately related to the actual physical processes by which permanent deformation, damage, and fracture occur.

C. Refine current relations

Incorporation of twinning into the constitutive relations, studies of other fcc and bcc materials, studies of other structure types (for example, hcp metals), the obtaining of more accurate constants for copper and iron through a systematic survey of available experimental data, and performing new experiments are all areas for future work.

D. Range of applicability of current relations

The current equations should be expected to apply at the very high strain rates and relatively low temperatures (by low we mean less than about one half the absolute melting temperature) which are described in the present study. For extremely high strain rates, the material deformation rate must become controlled by the rate of generating dislocations [as mentioned previously in the discussion relating to Eq. (4)], and thus the constitutive relation will be changed in a fundamental way. For the opposite consideration of relatively low strain rates and temperatures above one half the melting temperature, an analysis must be made of diffusion and dynamic recovery processes which come into play. For example, one effect of the action of dynamic recovery would be to alleviate the internal stress build ups associated with the microstructural stress intensity, and thereby, to influence the importance of the grain-size effect which is incorporated into the present study. As a consequence, the total plastic flow, damage, and fracturing behavior should be greatly affected.

ACKNOWLEDGMENTS

The authors wish to acknowledge the invaluable assistance of Gordon R. Johnson of Honeywell, Inc, who provided us with original test data for several of the metals used in the cylinder tests as well as cylinder test results including photomicrographs. He also provided advice on using and modifying the EPIC-2 code. M. E. Taylor of the University of Maryland kindly provided enlargements of the photomicrographs revealing the presence of twins in the iron tests. We would also like to thank K. Kim of NSWC for useful discussions of code results. C. W. Dickinson and K. W. Reed of NSWC provided encouragement and support for the work.

APPENDIX A

Assuming that all the plastic deformation in the Taylor test occurs at the rigid boundary, we can equate the rate of change of length of the cylinder to its velocity.

$$\frac{dL}{dt} = -u\,, \tag{A1}$$

and equate the deceleration of the cylinder to that produced by a force per unit area equal to the yield stress:

$$S = -\rho L \frac{du}{dt}\,. \tag{A2}$$

The solution of this pair of equations gives

$$\ln(L_1/L_0) = -\rho U^2/2S\,, \tag{A3}$$

where U is the intial velocity. If we denote $\ln(L_1/L_0)$ by ϵ_l (longitudinal strain) and use Eq. (2), we can write Eq. (A3) as

$$\epsilon_l + \epsilon_m = 0\,. \tag{A4}$$

This is the Taylor result in the limit of small impact velocities

(that is, for $\rho U^2/2S \ll 1$). In order to fit their data, Wilkins and Guinan used a modified form of Eq. (A3):

$$\ln[(L_1-h)/(L_2-h)] = -\tfrac{1}{2}\rho U^2/S, \qquad \text{(A5)}$$

which effectively moves the plastic shock front from the rigid boundary to a distance h from the rigid boundary. Using Wilkins simplified model, the duration of impact can be written

$$\frac{U\Delta t}{L_0} = 2\left(\frac{\rho U^2}{2S}\right)^{1/2} e^{-\rho U^2/2S}\int_0^{\sqrt{\rho U^2/2S}} e^{x^2}dx\,. \qquad \text{(A6)}$$

In the limit that $\rho U^2/2S \to 0$, both Eq. (A6) and Taylor's result reduce to

$$U\Delta t/L_0 \to 2(\rho U^2/2S)\,. \qquad \text{(A7)}$$

In order to obtain a rough estimate of the impact time for the purpose of doing a numerical simulation, the following approximation to the Taylor result can be used:

$$\frac{U\Delta t}{L_0} = \begin{cases} 2(\rho U^2/2S) & \text{for} \quad 0 < \rho U^2/2S < \frac{1}{8} \\ \rho U^2/2S & \text{for} \quad \frac{1}{8} < \rho U^2/2S < 1\,. \\ 1 & \text{for} \quad 1 < \rho U^2/2S \end{cases} \qquad \text{(A8)}$$

Equation (A8) gives results which are within 30% of the Taylor result. The worst case approximation occurs at the boundaries of the ranges. Note that for typical experiments, $0.3 < \rho U^2/2S < 0.7$, so that the approximation

$$\Delta t \sim (\rho U^2/2S)(L_0/U)$$

gives a reasonable estimate of the impact duration.

[1]G. R. Johnson and W. H. Cook, in *Proceedings of the Seventh International Symposium on Ballistics*, The Hague, The Netherlands, 1983, p. 541.

[2]G. R. Johnson and W. H. Cook, Eng. Fract. Mech. **21**, 31 (1985).

[3]We will use the term "hydrocode" to refer to any computer program which attempts to solve the equations of motion for the dynamics of any material, fluid or not.

[4]W. G. Johnston and J. J. Gilman, J. Appl. Phys. **30**, 129 (1959).

[5]U. F. Kocks, A. S. Argon, and M. F. Ashby, *Thermodynamics and Kinetics of Slip, Progress in Materials Science Vol.* 19 (Pergamon, Oxford, UK, 1975).

[6]G. I. Taylor, Proc. R. Soc. London A **194**, 289 (1948); A. C. Whiffin, *ibid.* **194**, 300 (1948).

[7]M. L. Wilkins and M. W. Guinan J. Appl. Phys. **44**, 1200 (1973).

[8]E. H. Lee and S. J. Tupper, J. Appl. Mech. **21**, 63 (1954).

[9]J. B. Hawkyard, D. Eaton, and W. Johnson, Int. J. Mech. Sci. **10**, 929 (1968).

[10]D. C. Erlich and P. Chartagnac, J. Phys. Colloq. C5, Suppl. 8, **46**, 455 (1985).

[11]E. Orowan, Proc. Phys. Soc. London **52**, 8 (1940).

[12]A. V. Granato, in *Metallurgical Effects at High Strain Rates*, edited by R. W. Rohde, B. M. Butcher, J. R. Holland, and C. H. Karnes (Plenum, New York, 1973), p. 255.

[13]Y. M. Gupta, J. Appl. Phys. **46**, 3395 (1975).

[14]R. W. Armstrong, Acta Metall. **15**, 667 (1967).

[15]R. W. Armstrong and J.D. Campbell, in *The microstructure and Design of Alloys, Proceedings of the Third International Conference on the Strength of Metals and Alloys Vol.* 1 (Inst. Metals and the Iron and Steel Inst., Cambridge, 1973), p. 529.

[16]H. Conrad, J. Iron Steel Inst. **198**, 364 (1961).

[17]Z. S. Basinski, Philos. Mag. **4**, 393 (1959).

[18]G. I. Taylor, Proc. R. Soc. London A **145**, 362 (1934); **145**, 388 (1934).

[19]J. F. Bell, Philos. Mag. **11**, 1135 (1965).

[20]R. W. Armstrong, in *Yield, Flow and Fracture of Polycrystals*, edited by T. N. Baker (Applied Science, London, 1983), p. 1.

[21]N. Hansen and B. Ralph, Acta Metall. **30**, 411 (1982).

[22]J. D. Campbell, R. H. Cooper, and T. J. Fischhof, in *Dislocation Dynamics*, edited by A. R. Rosenfield, G. T. Hahn, A. L. Bement, Jr., and R. I. Jaffee (McGraw-Hill, New York, 1968), p. 723.

[23]W. E. Carrington and M. L. V. Gaylor, Proc. R. Soc. London A **194**, 323 (1948).

[24]R. W. Armstrong and P. J. Worthington, in *Metallurgical Effects at High Strain Rates*, edited by R. W. Rohde, B. M. Butcher, J. R. Holland, and C. H. Karnes (Plenum, New York, 1974), p. 401.

[25]R. W. Rohde, Acta Metall. **17**, 353 (1969).

[26]R. H. Warnes, R. R. Karpp, and P. S. Follansbee, J. Phys. Colloq. C5 Suppl. 8, **46**, 583 (1985).

[27]C. Zener and J. H. Hollomon, J. Appl. Phys. **15**, 22 (1944).